Supplementary information: The role of the essential GTPase ObgE in regulating lipopolysaccharide synthesis in *Escherichia coli*

Liselot Dewachter, Babette Deckers, Israel Mares-Mejía, Elen Louwagie, Silke Vercauteren, Paul Matthay, Simon Brückner, Anna-Maria Möller, Franz Narberhaus, Sibylle C. Vonesch, Wim Versées, Jan Michiels

Supplementary Tables

Table S1: Nucleotide binding affinities (equilibrium dissociation constants, KD in µM) of wild-type and mutant ObgE proteins. Equilibrium dissociation constants (K_D) (± fitting error) were determined by isothermal titration calorimetry (ITC). The three right columns give the ratios of the K_D values for different nucleotides which represents the relative affinity for GTP compared to other nucleotides. NMB, no measurable binding.

	Equilibrium Dissociation Constants (µM)			Relative affinity for GTPγS		
Variant	K_D(GTPγS)	K_D(GDP)	K_D(ppGpp)	K_D(GDP)/ K_D(GTPγS)	K_D(ppGpp)/ K_D(GTPγS)	Reference
ObgE wt	1.3 ± 0.1	0.44 ± 0.03	0.63 ± 0.08	0.34	0.48	[1]
ObgE T174I	160 ± 11	115 ± 2	81 ± 3	0.72	0.51	[2]
ObgE D246G	14.8 ± 0.9	4.1 ± 0.4	7.8 ± 1.2	0.28	0.53	[1]
ObgE T193A	4.7 ± 0.4	0.53 ± 0.03	0.8 ± 0.1	0.11	0.17	[1]
ObgE E265K	5.7 ± 0.8	0.25 ± 0.03	0.31 ± 0.03	0.044	0.054	[2]
ObgE S270I	4.9 ± 0.5	0.45 ± 0.05	1.14 ± 0.09	0.092	0.23	[1]
ObgE N283I	NMB	NMB	NMB	NMB	NMB	[1]
ObgE D286Y	NMB	NMB	NMB	NMB	NMB	[1]

Table S2. Bacterial strains and plasmids used in this study.

***E. coli* strain**	**Details**	**Source**
BW25113	*lacI*$^+$ *rrnB*$_{T14}$ Δ*lacZ*$_{WJ16}$ *hsdR*514 Δ*araBAD*$_{AH33}$ Δ*rhaBAD*$_{LD78}$ *rph-1*	[3]
Δ*rcsA*	BW25113 Δ*rcsA*	[3]
Δ*rcsB*	BW25113 Δ*rcsB*	[3]
Δ*rcsF*	BW25113 Δ*rcsF*	[3]
Δ*recA*	BW25113 Δ*recA*	[3]
Δ*rnhB::Km*^{R}	BW25113 Δ*rnhB::Km*^{R}	[3]
Δ*wcaE*	BW25113 Δ*wcaE*	[3]
Δ*wcaJ*	BW25113 Δ*wcaJ*	[3]
lpxA$_{V197H}$	BW25113 *lpxA* 586-600 GGTGTCAATATCGAA > GGCCATAACATTGAG	This work
lpxA$_{I199S}$	BW25113 *lpxA* 596 T>G	This work
lpxA$_{R216C}$	BW25113 *lpxA* 646 C>T	This work
CFT073		From the lab of prof. Van Melderen, ULB, BE
DHM1	F$^-$ *cya*-854 *recA*1 *endA*1 *gyrA*96 (Nal^R) *thi*1 *hsdR*17 *spoT*1 *rfbD*1 *glnV*44(AS)	[4]
BL21(DE3) pLysS	F-*hsdS*B (rB$^-$mB$^-$) *gal dcm* (DE3) pLysS (Cm^R) ΔTonB	[5]
MG1655 *dcas9*	MG1655 Δ*araBAD ileY*::P$_{tet}$-*dcas9*	This work

Plasmid	Details	Source
pBAD33Gm	p15A ori, Gm^R, P_{BAD} promoter	[6]
pBAD33Gm-*obgE*	See pBAD33Gm, expression of *obgE*	[6]
pBAD33Gm-*obgE**	See pBAD33Gm, expression of $obgE_{K268I}$	[6]
pBAD33Gm-*obgE**-*venus*	See pBAD33Gm, expression of $obgE_{K268I}$-*venus*	[2]
pBAD33Gm-*obgE**$_{T174I}$	See pBAD33Gm, expression of $obgE_{K268I, T174I}$	[2]
pBAD33Gm-*obgE**$_{T193A}$	See pBAD33Gm, expression of $obgE_{K268I, T193A}$	[2]
pBAD33Gm-*obgE**$_{D246G}$	See pBAD33Gm, expression of $obgE_{K268I, D246G}$	[2]
pBAD33Gm-*obgE**$_{E265K}$	See pBAD33Gm, expression of $obgE_{K268I, E265K}$	[2]
pBAD33Gm-*obgE**$_{S270I}$	See pBAD33Gm, expression of $obgE_{K268I, S270I}$	[2]
pBAD33Gm-*obgE**$_{N283I}$	See pBAD33Gm, expression of $obgE_{K268I, N283I}$	[2]
pBAD33Gm-*obgE**$_{D286Y}$	See pBAD33Gm, expression of $obgE_{K268I, D286Y}$	[2]
pCA24N-*lpxA*	ColE1 ori, Cm^R, expression of *lpxA* from P-T5-*lac*	[7]
pET28a	ColE1 ori, Km^R, expression from P-T7-*lac*	Novagen
pET28a-*obgE*	See pET28a, expression of *obgE*	[8]
pET28a-*obgE**	See pET28a, expression of $obgE_{K268I}$	This work
pET28a-*lpxA*	See pET28a, expression of *lpxA*	This work
pET28a-$lpxA_{V197H}$	See pET28a, expression of $lpxA_{V197H}$ (*lpxA* 589-591 GTC > CAT)	This work
pET28a-$lpxA_{I199S}$	See pET28a, expression of $lpxA_{I199S}$	This work
pET28a-$lpxA_{R216C}$	See pET28a, expression of $lpxA_{R216C}$	This work
pKT25	p15A ori, Km^R, expression of T25 from P_{lac}	[4]
pKT25-*lpxA*	See pKT25, expression of T25-*lpxA*	[9]
pKT25-*obgE*	See pKT25, expression of T25-*obgE*	This work
pKT25-*zip*	See pKT25, expression of T25-*zip*	[4]
pKNT25	p15A ori, Km^R, expression of T25 from P_{lac}	[4]
pKNT25-*lpxA*	See pKNT25, expression of *lpxA*-T25	[9]
pKNT25-*obgE*	See pKNT25, expression of *obgE*-T25	This work
pLC143	Integrative plasmid carrying P_{tet}-*dcas9*	[10]
pMDeg02	ColE1 ori, Ap^R, expression of *sfTq2* and *mCherry* from P_{trc}	[11]
pMS201-P_{rcsA}-*gfp*	pSC101 ori, Km^R, expression from P_{rcsA}	[12]
pQE80L	ColE1 ori, Km^R, expression from P-T5-*lac*	[13]
pQE80L-*obgE**-*mCherry*	See pQE80L, expression of $obgE_{K268I}$-*mCherry*	This work
pTargetF_lac_sgRNA	pMB1 ori, Ap^R, backbone of sgRNA library	[14]
pTargetF_lac_*ftsH*-531	Library plasmid encoding sgRNA 531 targeting *ftsH*	[14]
pTargetF_lac_*obgE*-271	Library plasmid encoding sgRNA 271 targeting *obgE*	[14]
pTargetF_lac_*obgE*-398	Library plasmid encoding sgRNA 398 targeting *obgE*	[14]
pTargetF_lac_*obgE*-436	Library plasmid encoding sgRNA 436 targeting *obgE*	[14]
pTargetF_lac_*obgE*-643	Library plasmid encoding sgRNA 643 targeting *obgE*	[14]
pTargetF_lac_*yciM*-641	Library plasmid encoding sgRNA 641 targeting *yciM*	[14]
pUT18	pMB1 ori, Ap^R, expression of T18 from P_{lac}	[4]
pUT18-*lpxA*	See pUT18, expression of *lpxA*-T18	[9]
pUT18-*obgE*	See pUT18, expression of *obgE*-T18	This work
pUT18C	pMB1 ori, Ap^R, expression of T18 from P_{lac}	[4]
pUT18C-*lpxA*	See pUT18C, expression of T18-*lpxA*	[9]
pUT18C-$lpxA_{V197H}$	See pUT18C, expression of T18-$lpxA_{V197H}$	This work
pUT18C-$lpxA_{I199S}$	See pUT18C, expression of T18-$lpxA_{I199S}$	This work
pUT18C-$lpxA_{R216C}$	See pUT18C, expression of T18-$lpxA_{R216C}$	This work
pUT18C-*obgE*	See pUT18C, expression of T18-*obgE*	This work
pUT18C-*zip*	See pUT18C, expression of T18-*zip*	[4]
pZE1-P_{dps}-*gfp*	ColE1 ori, Ap^R, expression from P_{dps}	[15]

Table S3: Primers used in this study

Primer	Sequence
BD1	GGTATACCATATGATTGATAAATCCGCCTTTGTGC
BD2	CCGGAATTCTTATTAACGAATCAGACCGCGCG
LD1	TTGGCGACAATACGGCGGTTG
LD2	CCCAGACTGACGGACTGACGTAATG
LD3	TCTTTTGTTCGCCAAACTTTACGGCC
LD4	CCGGGAAGTGTTCTTCATAAAACGCG
P209	AAAAAGGATCCAATGAAGTTTGTTGATGAAGCATCG
P210	AAAAAGGTACCCGTTTATCATCAGTGATTAACGC
P211	AAAAAGGATCCATGAAGTTTGTTGATGAAGCATCG
P212	AAAAAGGTACCCGACGCTTGTAAATGAACTCAACG
P213	GTGAGGCGATTACCGCTATCTGCAATGCGTATAAGCTG
P214	GATAGCGGTAATCGCCTC
P215	CAACGCCGTTCGGTGTCAATAGCGAAGGGCTGAAGCGC
P216	ATTGACACCGAACGGCGTTG
P217	GCCGTTCGGTCATAATATCGAAGGGCTGAAGCGC
P218	CGATATTATGACCGAACGGCGTTGCGTG
SPI10499	CTACTGTTTCTCCATACCCG
SPI10500	TGTTTTATCAGACCGCTTCT
SPI11124	CTGGAAATATACAGCCAGGATCTG
SPI11125	CTGGCTGTATATTTCCAGCTCG

Supplementary Figures

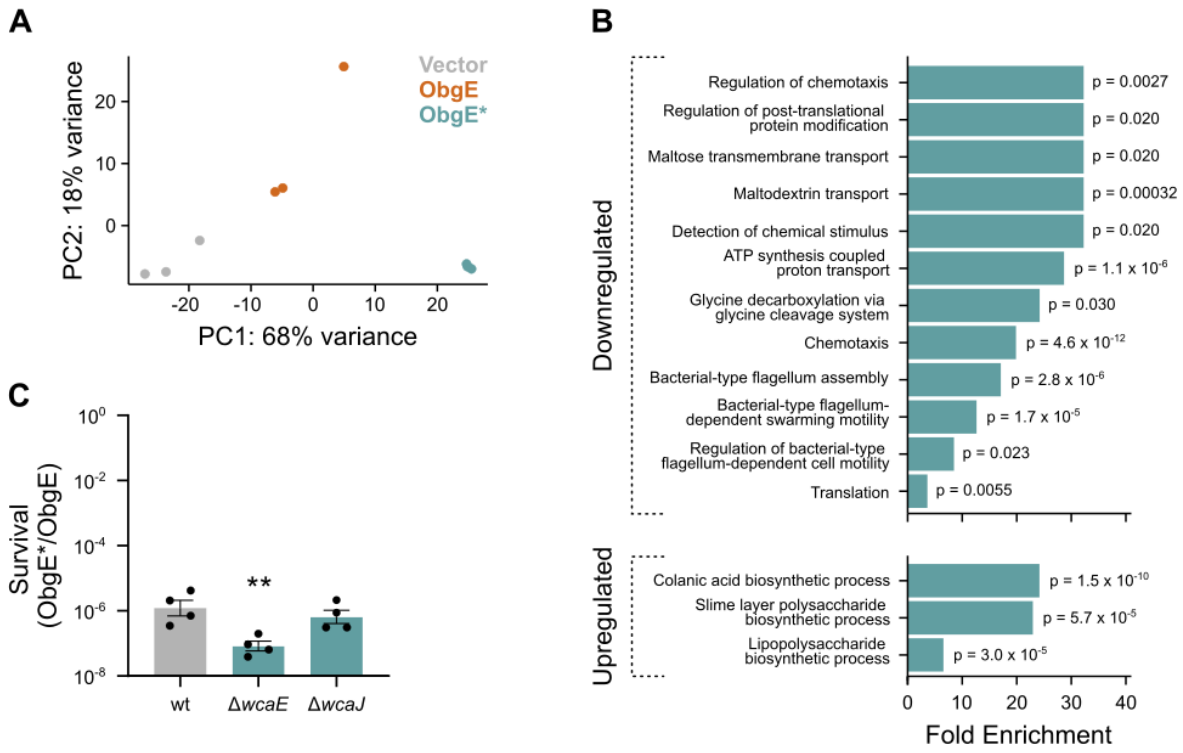

Figure S1: The toxic ObgE isoform, ObgE*, induces the Rcs stress response. A) RNA-seq analysis was performed on *E. coli* cultures containing pBAD33Gm (Vector), pBAD33Gm-*obgE* (ObgE) and pBAD33Gm-*obgE** (ObgE*) after 1h of induction with arabinose. The principal component analysis is plotted here. B) GO enrichment analyses for biological processes that are significantly affected by ObgE* were performed. Enrichment was determined by Fisher's exact tests starting from all genes that were downregulated (top) or upregulated (bottom) by ObgE* in comparison to both the Vector and ObgE samples. P values were FDR adjusted and all significantly over- or underrepresented categories are listed in Supplementary data 1. Here, the most specific overrepresented categories, their fold enrichment and corresponding FDR-adjusted p values are displayed. C) ObgE* toxicity is not decreased in the absence of colanic acid production. *E. coli* wt and colanic acid synthesis mutant cultures carrying pBAD33Gm-*obgE* or pBAD33Gm-*obgE** were induced with arabinose to activate *obgE(*)* expression. Two hours after induction, CFUs/ml were determined and the level of survival was calculated by dividing CFUs/ml upon *obgE** expression by those recorded upon wt *obgE* overexpression. Bar graphs and error bars represent the mean ± SEM, number of biological replicates n = 4. Ordinary one-way ANOVA with Dunnett's multiple comparisons test was performed against the wt control condition, ** $p < 0.01$.

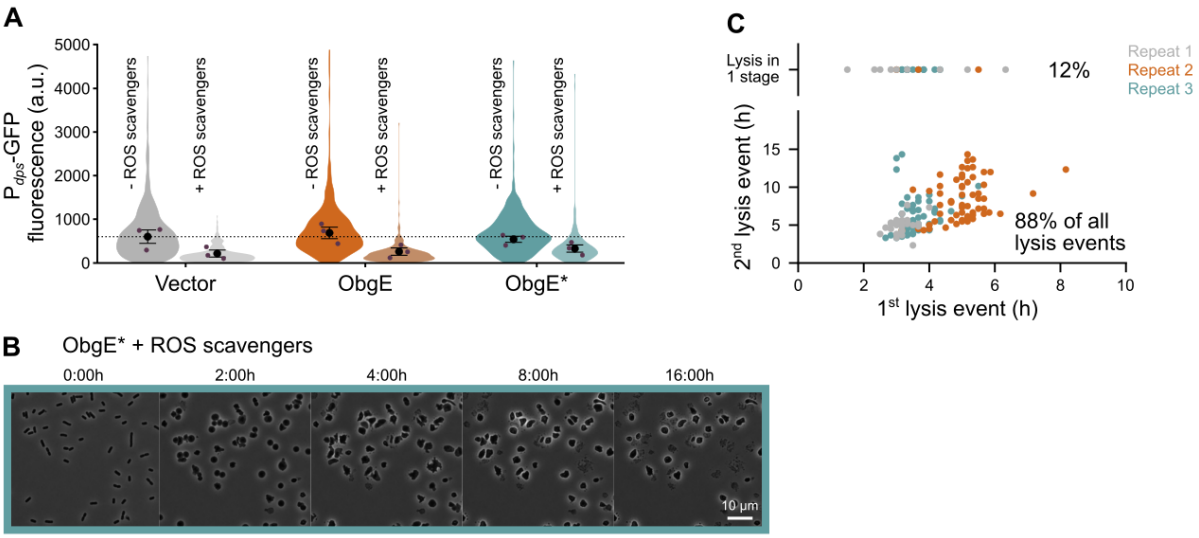

Figure S2: ObgE* toxicity in *E. coli* L-forms is unrelated to ROS production. A) ObgE* does not lead to higher ROS concentration in *E. coli* L-forms and a mixture of ROS scavengers (10 mM sodium pyruvate, 0.5% DMSO, 100 µM MnTBAP) is capable of lowering ROS concentrations in all three conditions (Vector, ObgE, ObgE*) similarly. Quantitative analysis was performed on microscopy images of *E. coli* pBAD33Gm (Vector), pBAD33Gm-*obgE* (ObgE) or pBAD33Gm-*obgE** (ObgE*) L-forms that also contain the pZE1-P_{dps}-GFP ROS reporter plasmid and that were grown in the presence or absence of ROS scavengers. This analysis revealed that ROS concentrations are lowered by the addition of scavengers and are not increased by *obgE** expression. ROS concentrations were estimated based on the GFP fluorescence of each L-form. L-form GFP fluorescence was corrected for cell size and background fluorescence. Data are represented as violin plots with the median GFP fluorescence of each repeat indicated with purple dots. Black dots and error bars represent the mean ± SEM of the recorded median values of each repeat, number of biological replicates n = 3, where each repeat contains > 50 L-forms. A one-way ANOVA on samples without ROS scavengers and on samples with ROS scavengers did not detect any statistical differences across the different conditions (p = 0.7156 and 0.6389, respectively). B) ObgE* inhibits proliferation of *E. coli* L-forms also when grown in the presence of scavengers that are capable of lowering ROS levels. Time lapse images of *E. coli* cells that express *obgE** in the presence of ROS scavengers are shown as they transition into the L-form stage and subsequently fail to proliferate. C) For L-forms expressing *obgE**, the frequency of the 2-stage lysis phenotype was quantified and the timing of the first and second lysis events was recorded.

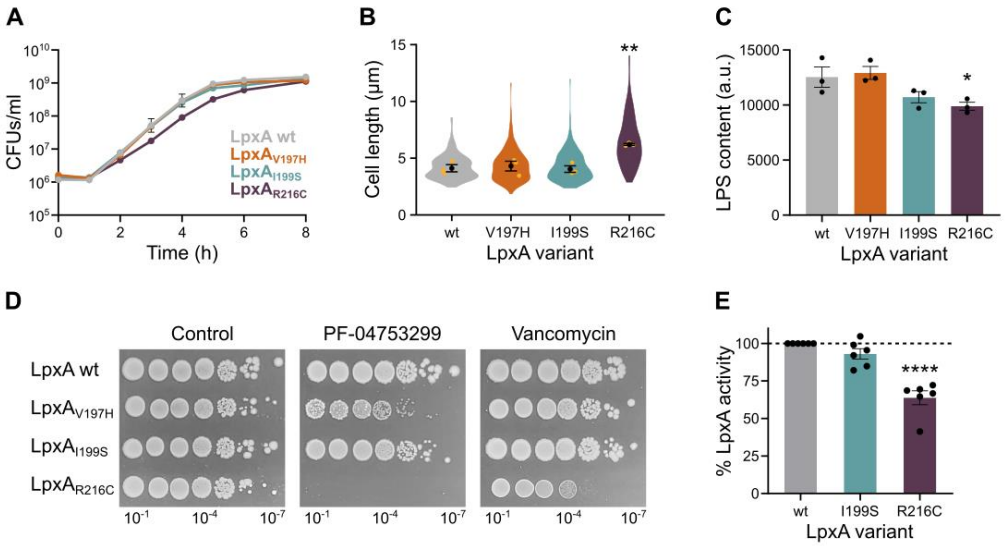

Figure S3: Selected *lpxA* mutants have little to no effects on LpxA activity, LPS synthesis, growth and morphology. A) *E. coli* *lpxA*$_{R216C}$, but not the other *lpxA* mutants, displays a slight growth defect. CFUs/ml of *E. coli* wt or *lpxA* V197H, I199S or R216C were monitored for a growth period of 8 hours. Data are represented as the mean ± SEM, number of biological replicates n ≥ 4. B) *E. coli* *lpxA*$_{R216C}$, but not the other *lpxA* mutants, has an increased cell length, as determined by quantitative microscopy after 3 hours of growth. Yellow dots represent the median cell length recorded in each biological repeat. Black dots and error bars represent the mean of the recorded medians ± SEM, number of biological replicates n = 3. Ordinary one-way ANOVA with Dunnett's multiple comparisons test was performed to compare against the wt control condition, ** $p < 0.01$. C) *E. coli* *lpxA*$_{R216C}$, but not the other *lpxA* mutants, shows a significant decrease in LPS content. Bar graphs and error bars represent the mean ± SEM, number of biological replicates n = 3. Ordinary one-way ANOVA with Dunnett's multiple comparisons test was performed against wt as control condition, * $p < 0.05$. D) Selected *lpxA* mutants display alterations in sensitivity to different compounds. A 10-fold dilution series of overnight cultures of *E. coli* wt or *lpxA* V197H, I199S or R216C was plated on medium without compounds (Control) or with the LPS inhibitor PF-04753299 or the cell wall targeting antibiotic vancomycin. Because vancomycin is unable to penetrate the outer membrane, sensitivity to this antibiotic hints at outer membrane defects. E) LpxA$_{R216C}$ displays decreased enzymatic activity. *In vitro* LpxA activity assays were performed and recorded signals were normalized to wt LpxA. Data are represented as mean ± SEM, number of biological replicates n = 6. Ordinary one-way ANOVA with Dunnett's multiple comparisons test was performed to compare against the wt control condition, **** $p < 0.0001$.

A

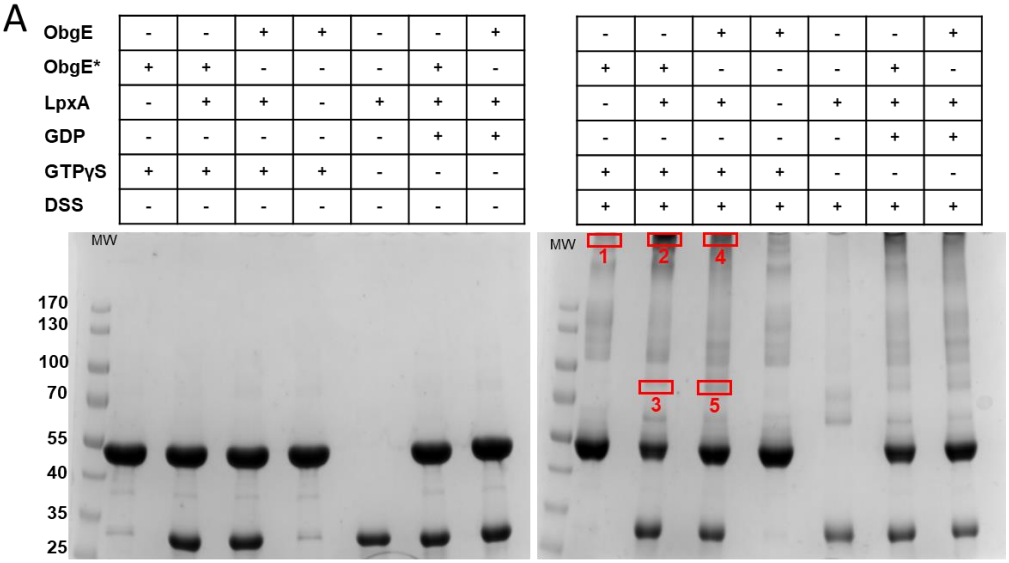

B

Protein composition	MW [kDa]	#Peptides	SC* [%]	FragCov** [%]
Band 1				
ObgE	45,4	19	51	18,3
Band 2				
ObgE	45,4	14	38,5	13,7
LpxA	30,2	9	31,2	2,8
Band 3				
ObgE	45,4	16	40,2	23,2
LpxA	30,2.	5	21,3	2,5
Band 4				
ObgE	45,4	21	50,5	23,2
LpxA	30,2	12	35,8	2,5
Band 5				
ObgE	45,4	19	46,8	22,9
LpxA	30,2	8	28,4	3,9

*Sequence Coverage
** Fragment Coverage

Figure S4: Crosslinking and MS analysis of the ObgE-LpxA and ObgE*-LpxA complexes. A) SDS-PAGE analysis of the complexes formed between LpxA and either ObgE or ObgE* after crosslinking with disuccinimidyl suberate (DSS). The analysis was performed with ObgE/ObgE* either bound to GDP or GTPgS. Crosslinking of the individual LpxA, ObgE and ObgE* proteins was used as a control. As a reference also the corresponding non-crosslinked samples were analyzed on SDS-PAGE (left gel). The bands indicated with a red box were excised for MS analysis. B) Table summarizing the results of the MS analysis of the bands excised from the SDS-PAGE shown in panel A (red boxes). The bands were excised, and the proteins digested with trypsin according to the proteaseMax manufacturers protocol and analyzed with MALDI-TOF/TOF.

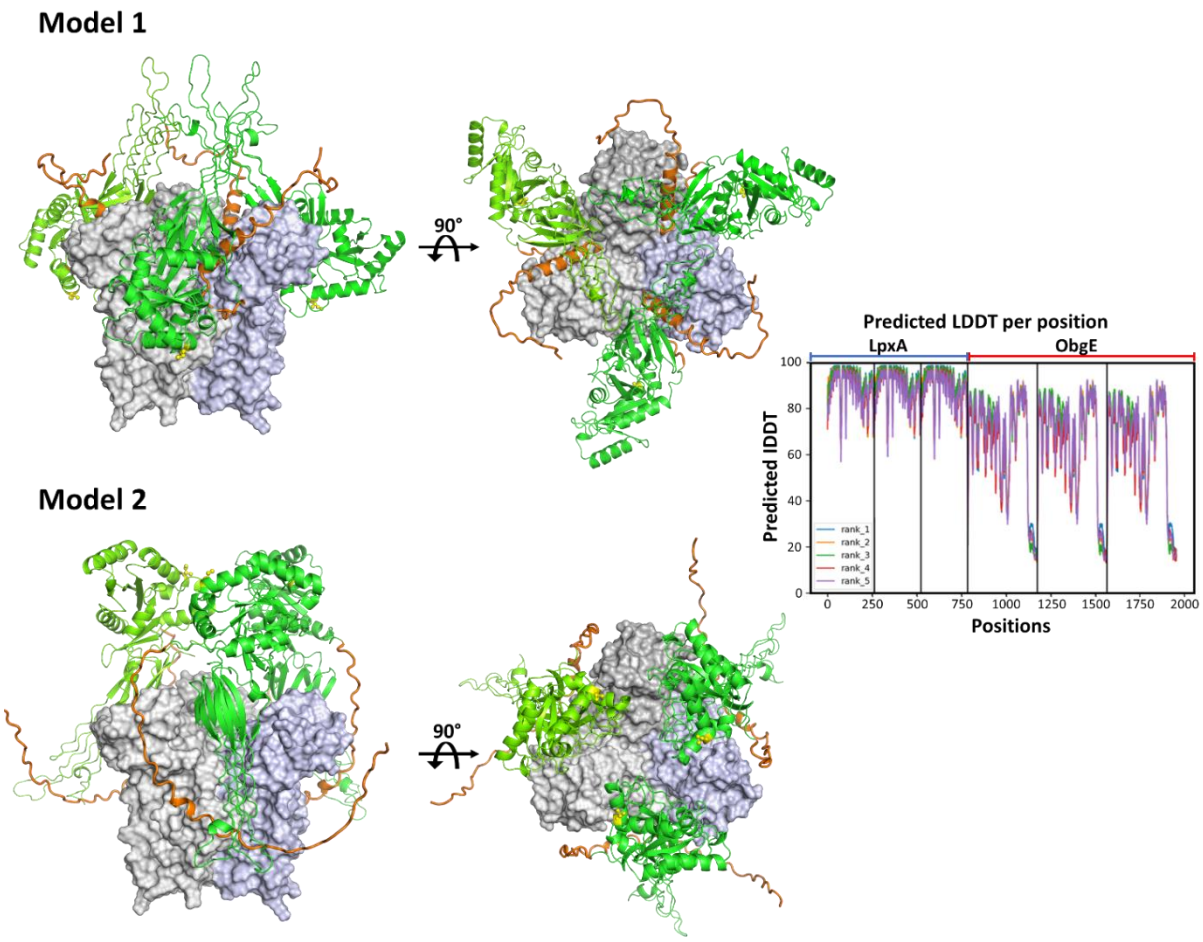

Figure S5: AlphaFold models of the LpxA-ObgE* complex. The two highest ranked models ("model 1" and "model 2") predicting the binding interaction mode of 3 ObgE* molecules to an LpxA trimer are shown. LpxA is shown in surface representation with each of the subunits in a different shade of grey, while ObgE* is shown in green (G domain and N-terminal domain) and orange (C-terminal domain). The position of the K268I mutation is indicated in yellow sticks. The inset plot shows the predicted LDDT per position.

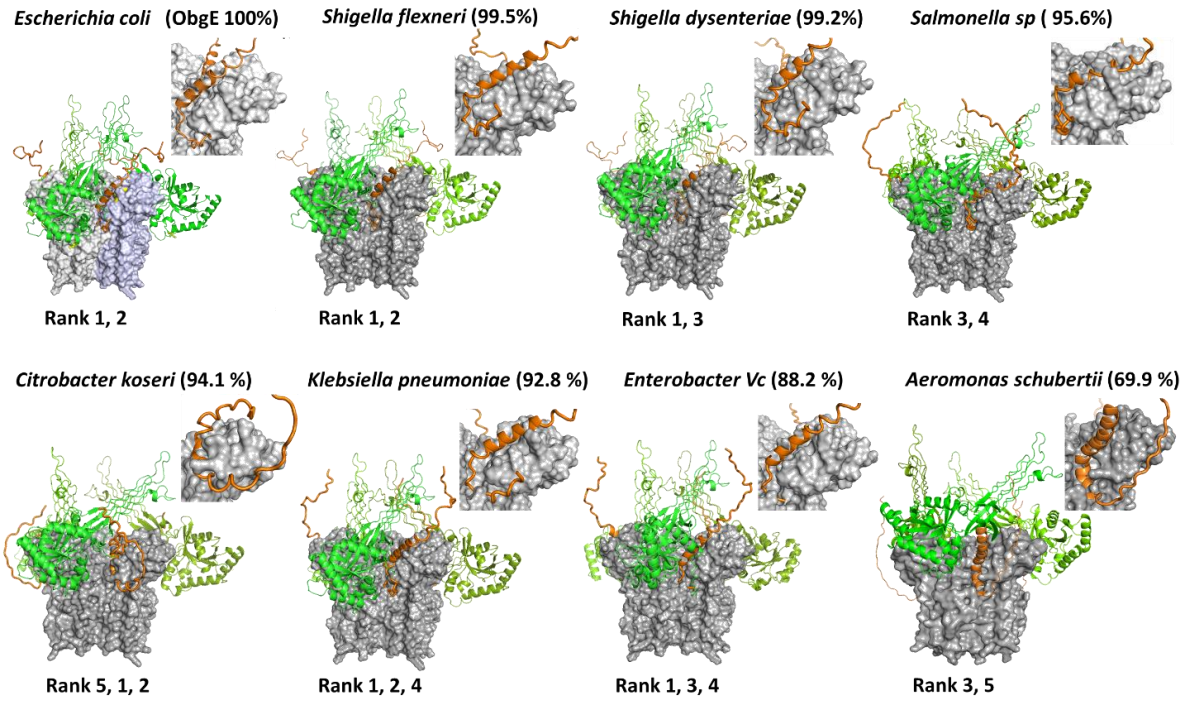

UNIPROT codes for all sequences used.

	Obg	LpxA
Escherichia coli	P42641	P0A722
Shigella flexneri	Q0T0A1	Q0T828
Shigella dysenteriae	Q32BF0	Q32JS8
Salmonella sp	WP_192513500.1	B4TYE1
Citrobacter koseri	A0A381GXD2	A0A381H7L8
Klebsiella pneumoniae	A6TEK2	A6T4Y3|
Enterobacter Vc	WP_220267381.1	WP_220267606.1
Aeromonas schubertii	A0A0W7TWA3	A0A0W7U3W8

Figure S6: AlphaFold models of the complexes formed between representatives of Obg and LpxA from the class of *Gammaproteobacteria*. The sequence identity between the respective Obg proteins and the *E. coli* ObgE is indicated in between brackets. In all cases, binding modes that are very similar to Model 1 are obtained among the top 5 ranked models (the rank of the models similar to Model 1 are indicated below each structure model). The insets show a close-up view of the interaction between the C-terminal tail of Obg and LpxA.

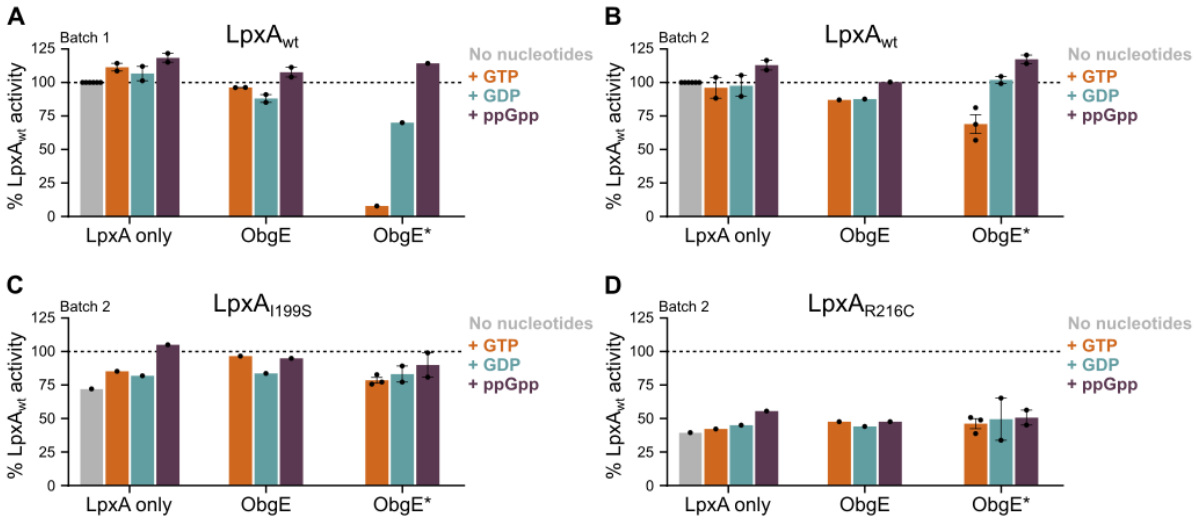

Figure S7: The effect of ObgE and ObgE* on LpxA activity. A) The effect of ObgE or ObgE* (125 nM) on the activity on LpxA$_{wt}$ was determined in the presence of different nucleotides, using batch 1 of substrates and purified proteins. Results were normalized to the activity of LpxA$_{wt}$ without the addition of ObgE(*) or nucleotides. Data are represented as mean ± SEM, number of biological replicates n ≥ 1. No statistical tests were performed. B-D) The effect of ObgE or ObgE* (7 nM) on the activity on LpxA$_{wt}$, LpxA$_{I199S}$, or LpxA$_{R216C}$ was determined in the presence of different nucleotides, using batch 2 of substrates and purified proteins. Results were normalized to the activity of LpxA$_{wt}$ without the addition of ObgE(*) or nucleotides. Data are represented as mean ± SEM, number of biological replicates n ≥ 1. No statistical tests were performed.

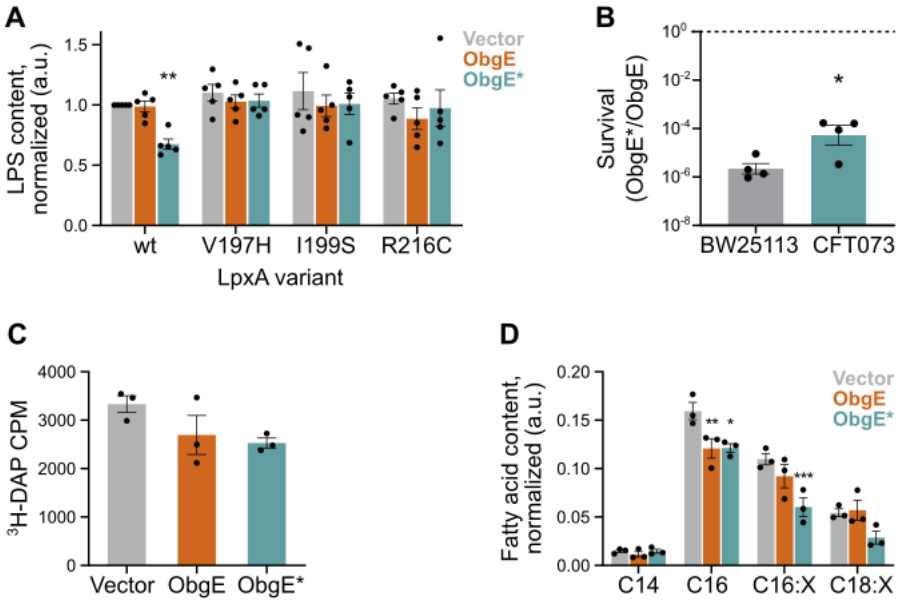

Figure S8: The inhibition of LpxA by ObgE* lowers LPS levels but does not increase peptidoglycan or fatty acid production. A) ObgE* no longer decreases cellular LPS content in the presence of *lpxA* mutations that provide resistance to ObgE*. Quantitative interpretation of gel-based LPS assays shows the amount of LPS present in each condition. Bar graphs and error bars represent the mean ± SEM, number of biological replicates n = 5. A one sample t test was performed to assess which samples display a normalized LPS content that deviates from one, ** $p < 0.01$. B) ObgE* remains toxic in *E. coli* CFT073, an *E. coli* strain that produces the LPS O-antigen. Exponential-phase cultures of each of these strains carrying pBAD33Gm-*obgE* or pBAD33Gm-*obgE** were induced with arabinose. Two hours after induction, CFUs/ml were determined and the level of survival was calculated by dividing CFUs/ml upon *obgE** expression by those recorded upon wt *obgE* overexpression. Bar graphs and error bars represent the mean ± SEM, number of biological replicates n = 4. An unpaired two-tailed t test was performed, * $p < 0.05$. C) ObgE or ObgE* do not change peptidoglycan synthesis. The production of peptidoglycan was monitored by measuring the incorporation of the radioactive label ^{3}H-DAP into newly synthesized cell wall. Bar graphs and error bars represent the mean ± SEM, number of biological replicates n = 3. Ordinary one-way ANOVA did not detect any significant differences, $p = 0.1493$. D) For some fatty acids, small decreases are caused by ObgE or ObgE*. Fatty acid concentrations were measured by gas chromatography (GC) and normalized by the total protein content found in each sample. Bar graphs and error bars represent the mean ± SEM, number of biological replicates n = 3. Ordinary one-way ANOVA with Sidak's multiple comparisons test was performed against the Vector control condition for each fatty acid species, * $p < 0.05$, ** $p < 0.01$, *** $p < 0.001$. CPM, counts per minute. DAP, diaminopimelic acid.

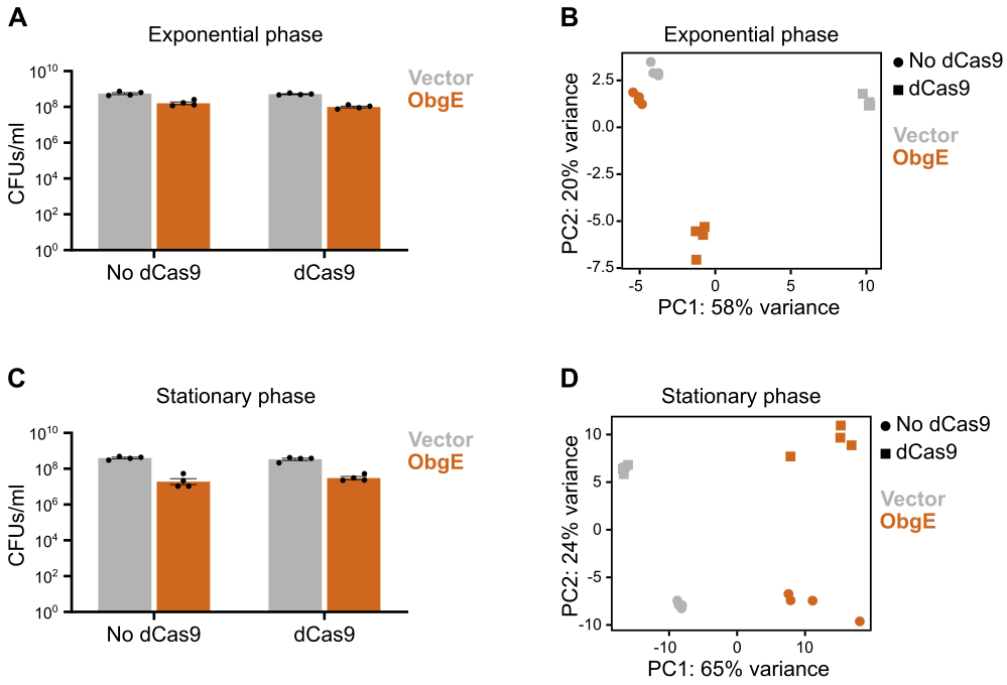

Figure S9: CRISPRi screens reveal several links between wt ObgE and the *E. coli* cell envelope. A) CFUs/ml at the time point of sampling the CRISPRi libraries in the exponential phase screen. Data are represented as mean ± SEM, number of biological replicates n = 4. B) Principal Component Analysis (PCA) plot for the CRISPRi screen performed in exponential phase. C) CFUs/ml at the time point of sampling the CRISPRi libraries in the stationary phase screen. Data are represented as mean ± SEM, number of biological replicates n = 4. D) PCA plot for the CRISPRi screen performed in stationary phase. PC, principal component.

Supplementary references

1. Verstraeten, N. *et al.* Biochemical determinants of ObgE-mediated persistence. *Mol. Microbiol.* 112, 1593–1608 (2019).
2. Dewachter, L. *et al.* GTP Binding Is Necessary for the Activation of a Toxic Mutant Isoform of the Essential GTPase ObgE. *Int. J. Mol. Sci.* 21, 16 (2019).
3. Baba, T. *et al.* Construction of Escherichia coli K-12 in-frame, single-gene knockout mutants: the Keio collection. *Mol. Syst. Biol.* 2, 2006.0008 (2006).
4. Karimova, G., Gauliard, E., Davi, M., Ouellette, S. P. & Ladant, D. Protein–Protein Interaction: Bacterial Two-Hybrid. in *Bacterial Protein Secretion Systems: Methods and Protocols* (eds. Journet, L. & Cascales, E.) 159–176 (Springer, New York, NY, 2017). doi:10.1007/978-1-4939-7033-9_13.
5. Weiner, M. P. *et al.* Studier pET system vectors and hosts. *Strateg Mol Biol* 7, 41–43 (1994).
6. Dewachter, L. *et al.* A Mutant Isoform of ObgE Causes Cell Death by Interfering with Cell Division. *Front. Microbiol.* 8, 1–12 (2017).
7. Kitagawa, M. *et al.* Complete set of ORF clones of Escherichia coli ASKA library (A Complete Set of E. coli K -12 ORF Archive): Unique Resources for Biological Research. *DNA Res.* 12, 291–299 (2005).
8. Gkekas, S. *et al.* Structural and Biochemical Analysis of *Escherichia coli* ObgE, a Central Regulator of Bacterial Persistence. *J. Biol. Chem.* 292, 5871-5883 (2017).
9. Möller, A.-M. *et al.* LapB (YciM) orchestrates protein–protein interactions at the interface of lipopolysaccharide and phospholipid biosynthesis. *Mol. Microbiol.* 119, 29–43 (2022).
10. Cui, L. *et al.* A CRISPRi screen in E. coli reveals sequence-specific toxicity of dCas9. *Nat. Commun.* 9, 1912 (2018).
11. Deghelt, M. *et al.* The outer membrane and peptidoglycan layer form a single mechanical device balancing turgor. *BioRxiv* 2023.04.29.538579 (2023).
12. Zaslaver, A. *et al.* A comprehensive library of fluorescent transcriptional reporters for Escherichia coli. *Nat. Methods* 3, 623–628 (2006).
13. Orman, M. A. & Brynildsen, M. P. Inhibition of stationary phase respiration impairs persister formation in E. coli. *Nat. Commun.* 6, 1–13 (2015).
14. Wang, T. *et al.* Pooled CRISPR interference screening enables genome-scale functional genomics study in bacteria with superior performance. *Nat. Commun.* 9, 2475 (2018).
15. Dwyer, D. J. *et al.* Antibiotics induce redox-related physiological alterations as part of their lethality. *Proc. Natl. Acad. Sci.* 111, E2100–E2109 (2014).